A Common Anesthetic Binding Site for Inhibition of Pentameric Ligand-gated Ion Channels

Monica N. Kinde, Ph.D., Weiming Bu, Ph.D., Qiang Chen, Ph.D., Yan Xu, Ph.D., Roderic G. Eckenhoff, M.D., Pei Tang, Ph.D.

Department of Anesthesiology, University of Pittsburgh School of Medicine (M.N.K., Q.C., Y.X. and P.T.); Department of Pharmacology and Chemical Biology, University of Pittsburgh School of Medicine (Y.X. and P.T.); Department of Structural Biology, University of Pittsburgh School of Medicine (Y.X.); Department of Computational and Systems Biology, University of Pittsburgh School of Medicine (P.T.); Department of Anesthesiology & Critical Care, University of Pennsylvania Perelman School of Medicine (W.B. and R.G.E.)

Supplementary Table S1. MS/MS analysis showing the two adducted peptides from the TMD region of ELIC: (**A**) ^{302}LAFPLGF*^{308} and (**B**) ^{256}LPYTTVIDQM*^{265}. The b and y ions identified are colored red and blue, respectively. The asterisk (*) indicates the residue containing a +216.076 Da (AziP*m*) modification. The far right column shows the delta mass.

Table S1A. The trypsin-digested adducted peptide AziP*m* ^{302}LAFPLGF*^{308} (MH+:980.510)

Residue	#	b ion	y ion	(1+)
L	1	114.1	980.5	7
A	2	185.1	867.5	6
F	3	332.2	796.4	5
P	4	429.3	649.3	4
L	5	542.3	552.3	3
G	6	599.4	439.2	2
F*	7	962.5	382.2	1

Table S1B. The trypsin-digested adducted peptide AziP*m* ^{256}LPYTTVIDQM*^{265} (MH+:1396.667)

Residue	#	b ion	y ion	(1+)
L	1	114.1	1396.7	10
P	2	211.1	1283.6	9
Y	3	374.2	1186.6	8
T	4	475.3	1023.5	7
T	5	576.3	922.4	6
V	6	675.4	821.4	5
I	7	788.5	722.3	4
D	8	903.5	609.2	3
Q	9	1031.5	494.2	2
M*	10	1378.7	366.2	1

Supplementary Figure S1. Total sequence coverage by MS/MS analysis for the AziP*m* photoaffinity labeling ELIC**.** 94% of the total ELIC sequence was recovered in the MS/MS analysis (residues in red) for the photoaffinity labeling of (**A**) ELIC in the absence of agonist and (**B**) ELIC in the presence of the agonist propylamine.

A

```
        10         20         30         40         50         60
APADNAADAR PVDVSVSIFI NKIYGVNTLE QTYKVDGYIV AQWTGKPRKT PGDKPLIVEN

        70         80         90        100        110        120
TQIERWINNG LWVPALEFIN VVGSPDTGNK RLMLFPDGRV IYNARFLGSF SNDMDFRLFP

       130        140        150        160        170        180
FDRQQFVLEL EPFSYNNQQL RFSDIQVYTE NIDNEEIDEW WIRGKASTHI SDIRYDHLSS

       190        200        210        220        230        240
VQPNQNEFSR ITVRIDAVRN PSYYLWSFIL PLGLIIAASW SVFWLESFSE RLQTSFTLML

       250        260        270        280        290        300
TVVAYAFYTS NILPRLPYTT VIDQMIIAGY GSIFAAILLI IFAHHRQANG VEDDLLIQRC

       310        320
RLAFPLGFLA IGCVLVIRGI TL
```

B

```
        10         20         30         40         50         60
APADNAADAR PVDVSVSIFI NKIYGVNTLE QTYKVDGYIV AQWTGKPRKT PGDKPLIVEN

        70         80         90        100        110        120
TQIERWINNG LWVPALEFIN VVGSPDTGNK RLMLFPDGRV IYNARFLGSF SNDMDFRLFP

       130        140        150        160        170        180
FDRQQFVLEL EPFSYNNQQL RFSDIQVYTE NIDNEEIDEW WIRGKASTHI SDIRYDHLSS

       190        200        210        220        230        240
VQPNQNEFSR ITVRIDAVRN PSYYLWSFIL PLGLIIAASW SVFWLESFSE RLQTSFTLML

       250        260        270        280        290        300
TVVAYAFYTS NILPRLPYTT VIDQMIIAGY GSIFAAILLI IFAHHRQANG VEDDLLIQRC

       310        320
RLAFPLGFLA IGCVLVIRGI TL
```

Supplementary Figure S2. Representative MS/MS spectra showing the peptides containing the AziP*m* adducted residues in the extracellular domain (ECD) under different functional states. Individual mass peaks are marked with either y- (red) or b- (black) ions, which correspond to the charge on the C- or N-terminus of the peptide, respectively. (**A**) An adducted residue Y102 in the ECD, labeled in the absence of agonist (the resting state of ELIC). Y102 was also labeled in the presence of agonist in a separate experiment. (**B**, **C**) AziP*m*-labeled residues in the presence of the agonist propylamine (a desensitized state) include (B) F95 and (C) G98. The identified peptide sequences are shown as insets.

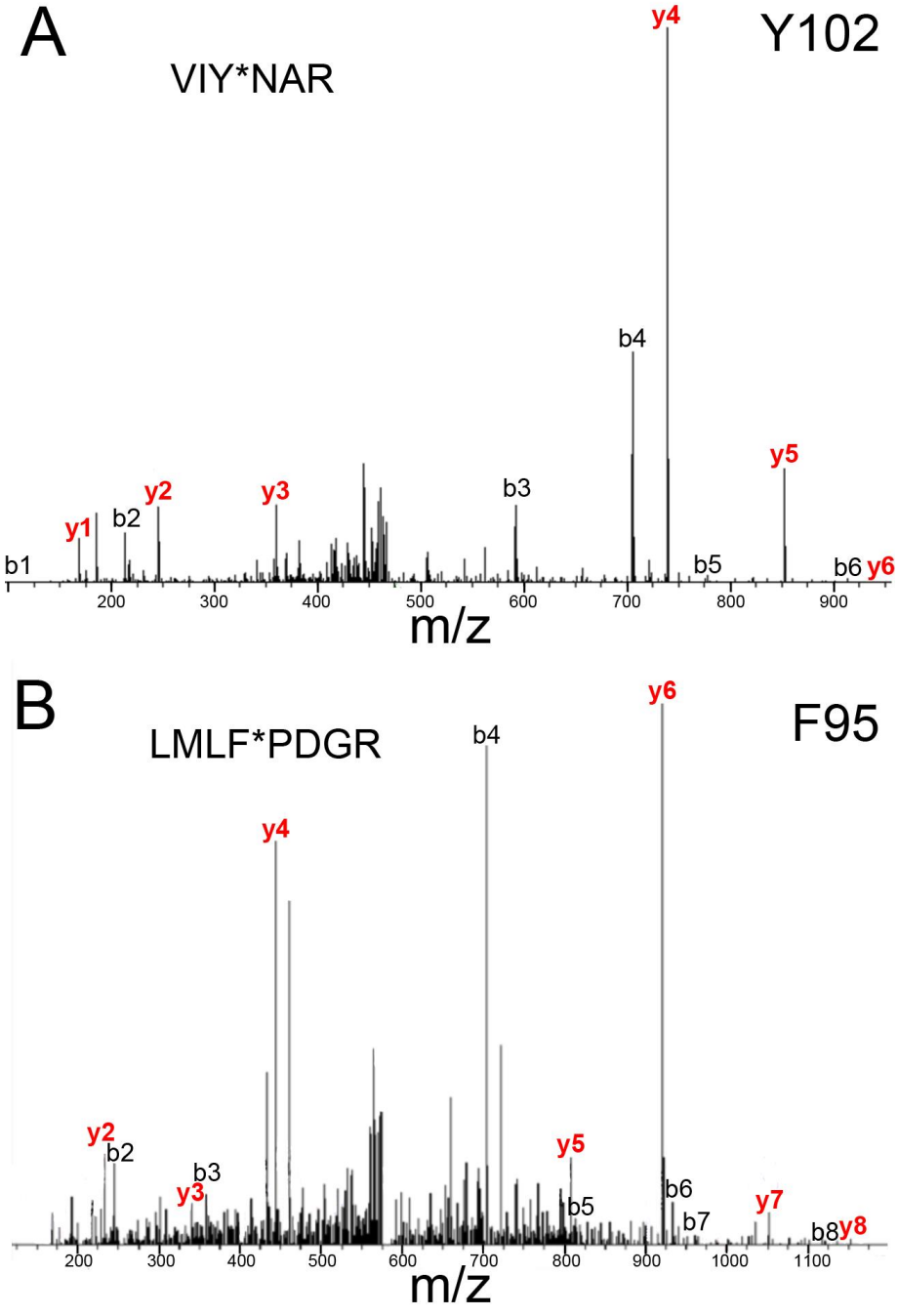

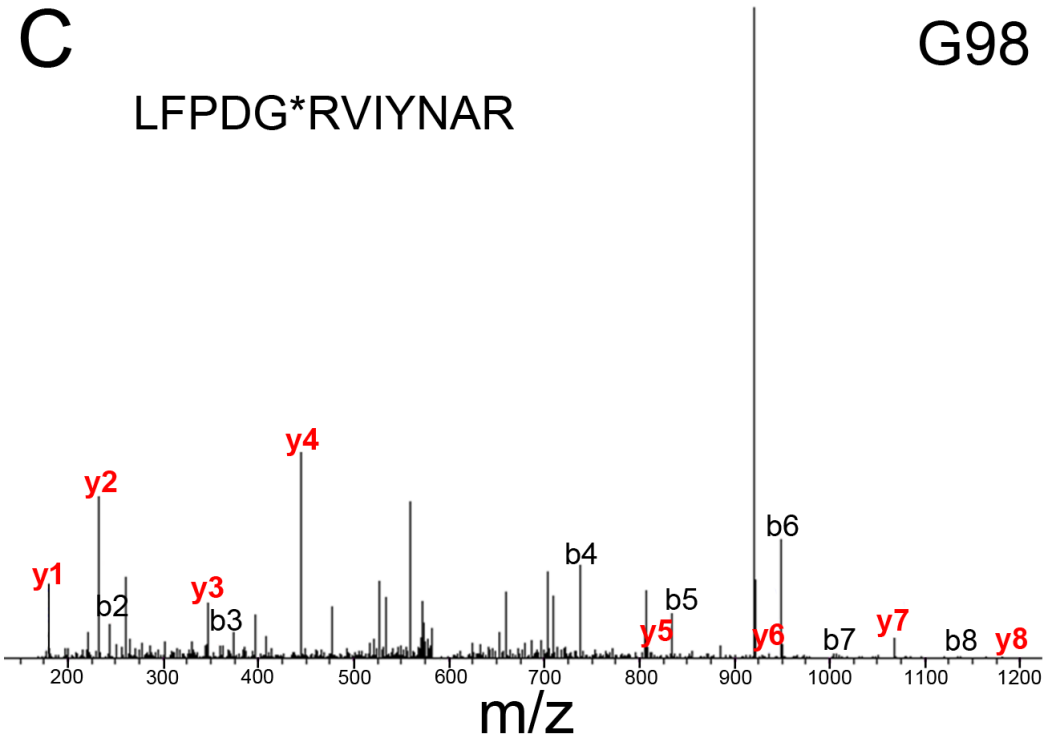
C
G98
LFPDG*RVIYNAR
y4
y2
y1
y3
b2
b3
b4
b6
b5
y5
y6
b7
y7
b8
y8
200
300
400
500
600
700
800
900
1000
1100
1200
m/z

Supplementary Figure S3. Anesthetics bind to an intra-subunit transmembrane domain (TMD) binding pocket. (**A**) In the current study, two ELIC residues in TM3 (M265) and TM4 (F308) are photolabeled by AziP*m*, a photoactivateable analogue of the anesthetic propofol. (**B**) Photolabeling experiments on GLIC with AziP*m* identified residues in TM1 (M205), TM3 (Y254) and TM4 (N307) that lined an intra-subunit TMD anesthetic binding site.[1] (**C**) Residues lining an equivalent intra-subunit binding pocket were found in close contact with propofol in the co-crystal structure of GLIC with propofol.[2] Propofol co-crystalized in the GLIC structure is shown in surface and licorice cyan. (**D**) Photoaffinity labeling of the δ subunit of nAChR from *Torpedo* with AziP*m*,[3] Halothane,[4] Azi-etomidate,[5] and TFD-etomidate.[6] (**E**) Sequence alignment of the three proteins shown in (A-D) showing homologous residues in the intra-subunit anesthetic binding pocket.

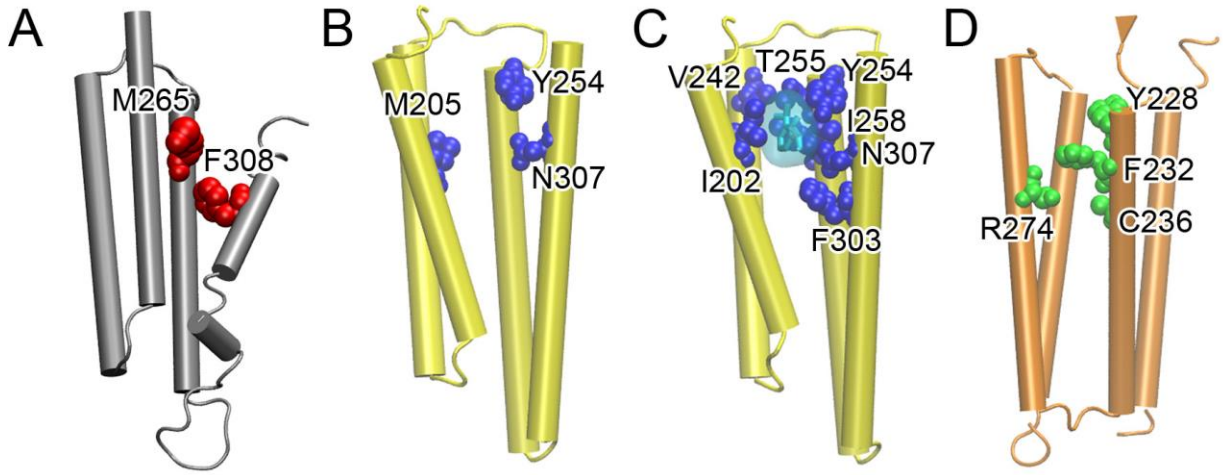

E

```
                                    TM1                                 TM2
  ELIC   183  PNQNEFSRITVRIDAVRNPSYYLWSFILPLGLIIAASWSVFWLES--FSERLQTSFTLMLTVVAYAFYTSNILPRLPYT-   259
  GLIC   177  -EDRLESKLDYQLRISRQYFSYIPNIILPMLFILFISWTAFWSTS--YEANVTLVVSTLIAHIAFNILVETNLPKTPYM-   252
δnAChR   207  PNGTNYQDVTFYLIIRRKPLFYVINFITPCVLISFLAALAFYLPA-ESGEKMSTAICVLLAQAVFLLLTSQRLPETALAV   285
                         TM3                                 TM4
  ELIC   260  TVIDQMIIAGYGSIFAAILLIIFAHHRQAN--GVEDDLLIQRCRLAFPLGFLAIGCVLVIRGITL----------------   322
  GLIC   253  TYTGAIIFMIYLFYFVAVIEVTVQHYLKVESQPARAASITRASRIAFPVVFLLANIILAFLFFGF----------------   317
δnAChR   286  PLIGKYLMFIMSLVTGVVVNCGIVLNFHFR--NLVGQTIDRLSMFIITPVMVLGTIFIFVMGNFNRPPAK----------   484
```

Supplementary Figure S4. [^{3}H]AziP*m* shares same binding sites with propofol. To determine whether propofol competes with AziP*m* for binding sites, we photolabeled ELIC with [^{3}H]AziP*m* (50 μM) in the absence and presence of 400 μM propofol, a concentration close to the maximum aqueous solubility of propofol. Counts per minute (CPM) results show a significant propofol inhibition of [^{3}H]AziP*m* binding, suggesting that propofol shares the same binding sites in ELIC with [^{3}H]AziP*m*. A mean CPM from three independent experiments with a standard error is presented for each labeling condition. T-test analysis was performed and showed that the presence and absence of propofol had made a significant difference for the [^{3}H]AziP*m* labeling (p=0.0053).

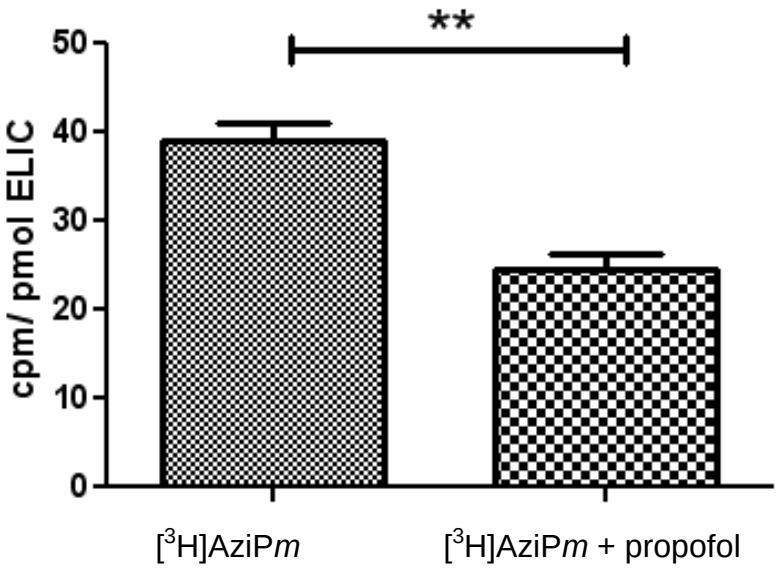

Supplementary Figure S5. (**A**) Single cysteine ELIC constructs, M265C and F308C, can be activated by the same agonist propylamine (PA) as used for the wild-type ELIC. Note that the F308C activation curve is almost identical to that of ELIC. (**B**) The TET-labeled M265C ELIC was reconstituted into lipid vesicles and injected into oocytes. The TET-labeled channels remain functional in both agonist (PA) elicited activation and propofol (PFL) inhibition. (**C**) The ELIC-α1β3GABA$_A$R chimera can be activated by the same agonist PA for ELIC activation (vertical axis on the left). The bar graph (vertical axis on the right) shows the propofol (20μM) potentiation of ELIC-α1β3GABA$_A$R at various concentrations of the agonist PA. The propofol potentiation effect gradually diminishes with increasing concentrations of PA. (**D**) Picrotoxin (PTX) and zinc (Zn) inhibit the ELIC-α1β3GABA$_A$R chimera.

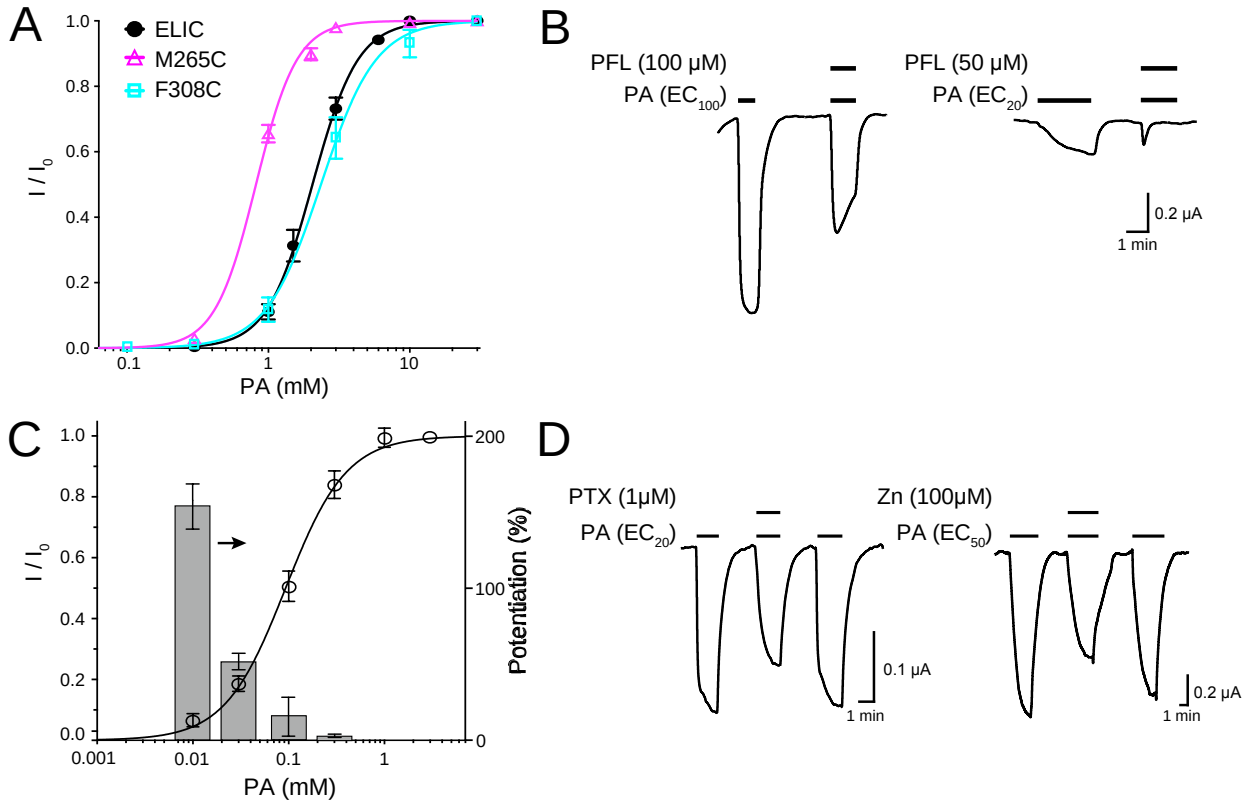

Supplementary Figure S6. Movement trajectories of propofol over the course of MD simulations. (**A** and **B**) Propofol initially bound to the TMD sites identified in the photolabeling experiments were stable over the course of two parallel MD simulations. Propofol trajectories in MD simulations are shown in both a top view (left panel) and a side view (right panel). Only one propofol molecule in subunit B in (A) had a large displacement. (**C** and **D**) Trajectories from two parallel simulations with propofol bound to the ECD sites suggested by photolabeling. The majority of propofol molecules were stable in the ECD sites over the simulations, with large displacements observed only at two sites near residues G98 (cyan) and F95 (green) in (D). For the convenience of visual comparison, the vertical scale for side view trajectories is kept the same for all the MD simulations (A – D). (**E**) Representative snapshots of stable propofol binding near residues Y102, G98, and F95. The representative docked propofol molecules near the three photolabeled ECD residues are shown in gray surfaces.

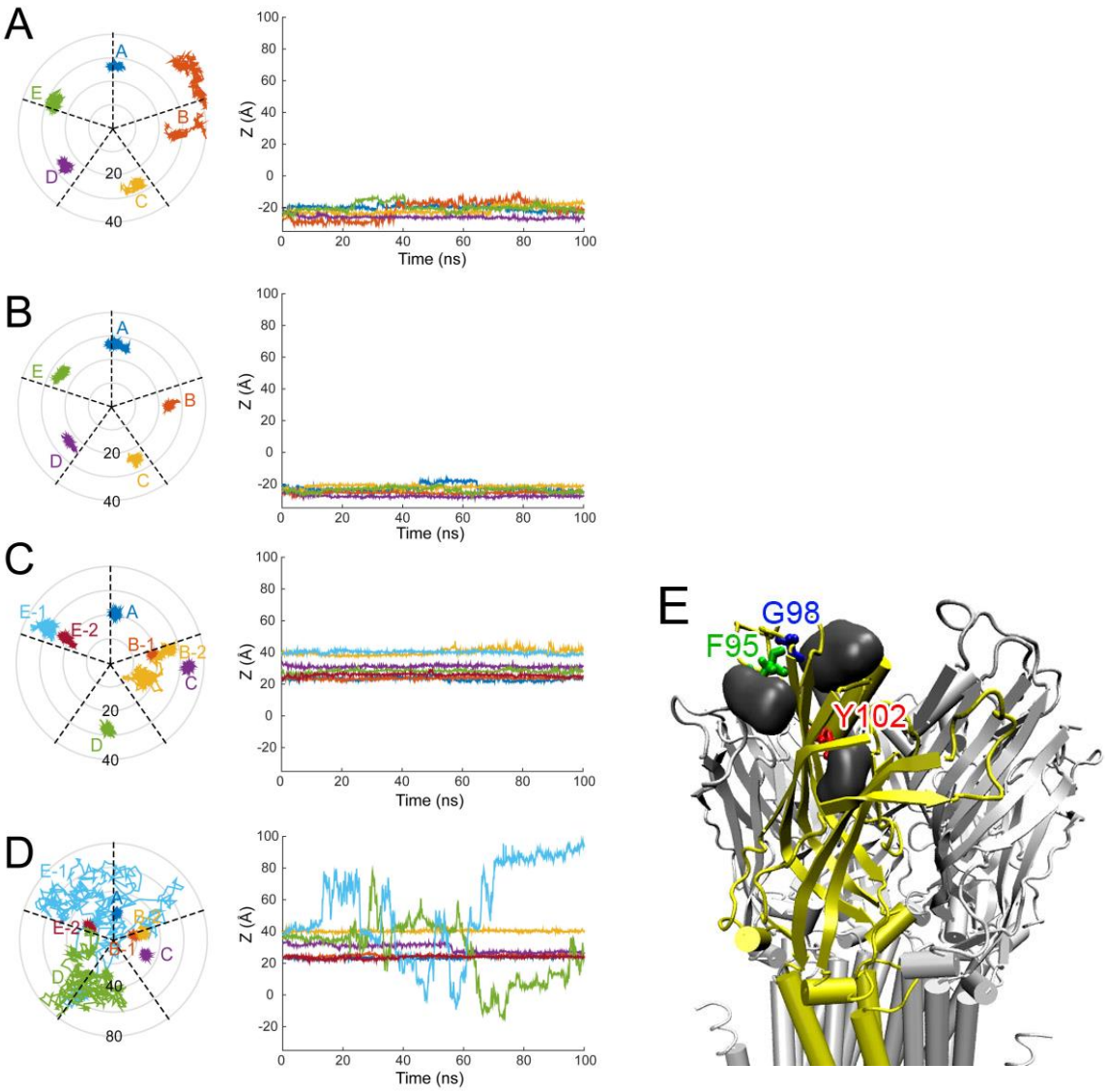

Supplementary Figure S7. Comparison of root mean square fluctuations (RMSFs) between APO ELIC and the propofol-bound ELIC. (**A**) RMSFs of APO ELIC (blue) and ELIC bound with propofol in the TMD (orange). Note the highlighted gray region showing the reduced RMSFs of ELIC upon propofol binding to the TMD intra-subunit pocket. (**B**) The observed decreases of RMSFs for the region highlighted in gray in (A) were determined to be statistically significant compared to the lower half of the TM3 helix (yellow region). Each dot represents the RMSF difference for a particular residue in the region. (**C**) RMSFs of APO ELIC (blue) and ELIC bound with propofol in the ECD (red). The region highlighted in gray is the same region as highlighted in (A), but does not show the same RMSF changes. (**D**) The same statistical analysis as used in (B) was performed on the data presented in (C), but no statistical difference in RMSFs was observed.

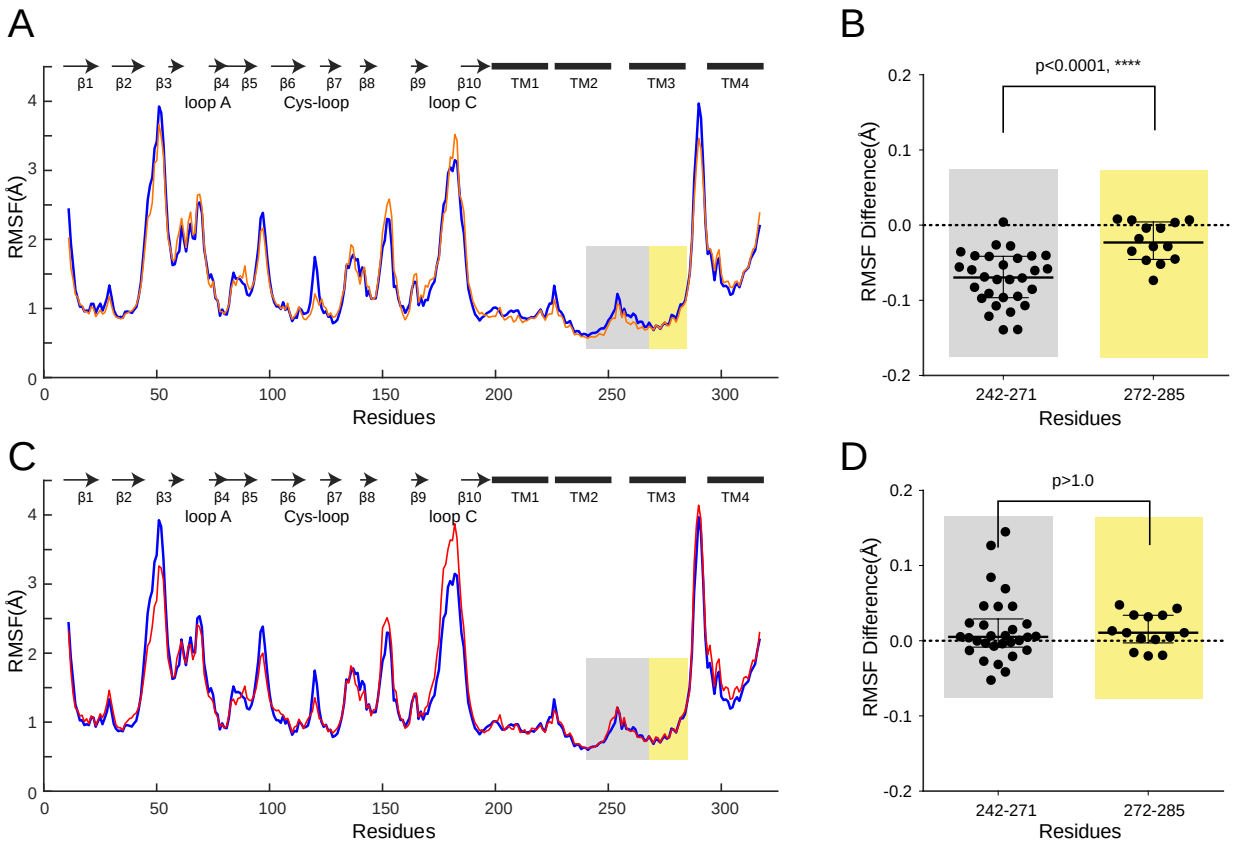

Supplementary Figure S8. Outward tilting of the transmembrane helix TM4 shown in overlaid transmembrane domain structures of APO and propofol-bound ELIC. (**A**) Side view and (**B**) top view of propofol binding to the intra-subunit pocket (orange) lined by M265 and F308 causes a 7° radial tilt of TM4 toward the lipid membrane relative to the APO ELIC (cyan). The plasticity of TM4 reacted to propofol binding is consistent with a higher RMSF of TM4 relative to RMSF values found in other TM helices (Figure S7).

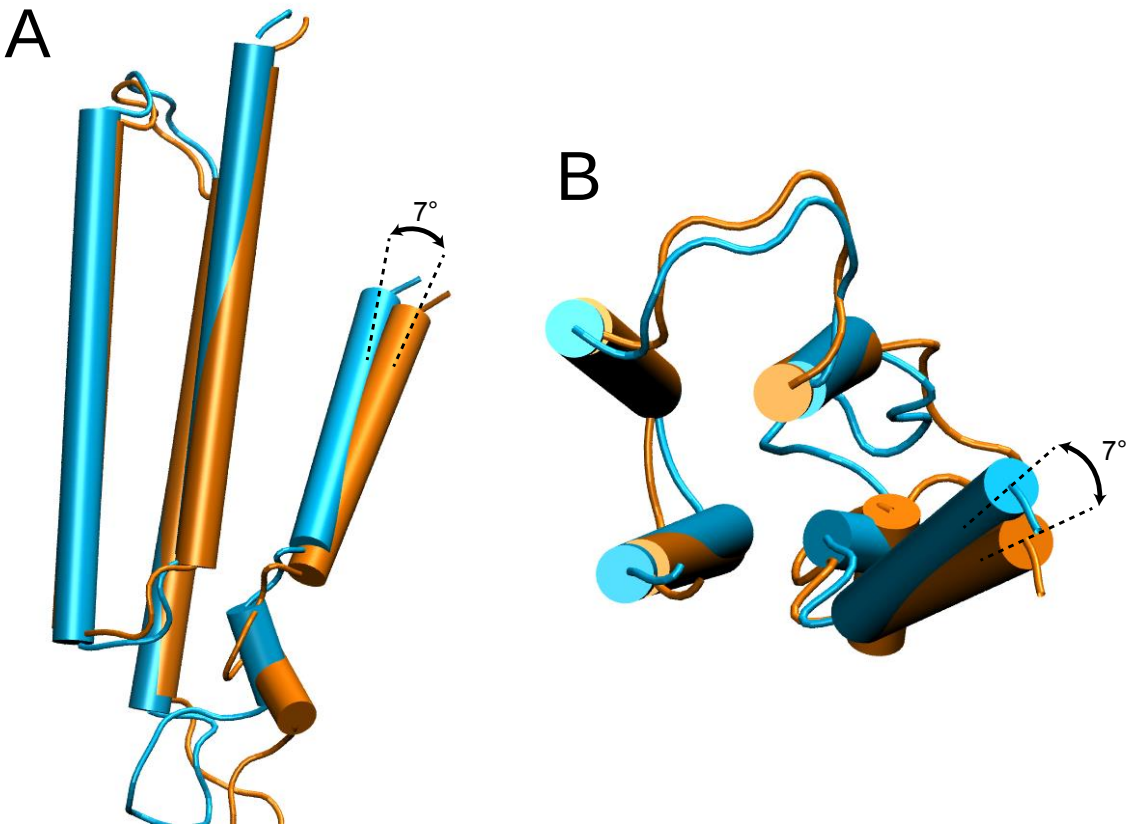

Supplementary Information References

1. Chiara DC, Gill JF, Chen Q, Tillman T, Dailey WP, Eckenhoff RG, Xu Y, Tang P, Cohen JB: Photoaffinity labeling the propofol binding site in GLIC. Biochemistry 2014; 53: 135-42
2. Nury H, Van Renterghem C, Weng Y, Tran A, Baaden M, Dufresne V, Changeux JP, Sonner JM, Delarue M, Corringer PJ: X-ray structures of general anaesthetics bound to a pentameric ligand-gated ion channel. Nature 2011; 469: 428-31
3. Jayakar SS, Dailey WP, Eckenhoff RG, Cohen JB: Identification of propofol binding sites in a nicotinic acetylcholine receptor with a photoreactive propofol analog. J Biol Chem 2013; 288: 6178-89
4. Chiara DC, Dangott LJ, Eckenhoff RG, Cohen JB: Identification of nicotinic acetylcholine receptor amino acids photolabeled by the volatile anesthetic halothane. Biochemistry 2003; 42: 13457-67
5. Chiara DC, Hong FH, Arevalo E, Husain SS, Miller KW, Forman SA, Cohen JB: Time-resolved photolabeling of the nicotinic acetylcholine receptor by [3H]azietomidate, an open-state inhibitor. Mol Pharmacol 2009; 75: 1084-95
6. Hamouda AK, Stewart DS, Husain SS, Cohen JB: Multiple transmembrane binding sites for p-trifluoromethyldiazirinyl-etomidate, a photoreactive Torpedo nicotinic acetylcholine receptor allosteric inhibitor. J Biol Chem 2011; 286: 20466-77